DE GRUYTER OPEN
10.1515/mecdc-2018-0006

PHYSICAL MODEL OF SI-ENGINE PROCESS AND GAS EXCHANGE FOR REAL-TIME IMPLEMENTATION IN ENGINE MANAGEMENT SYSTEM

JAN FOŘTL, JOHANNES BEER, JENS KELLER
Continental, Siemensstraße 12, D-93055 Regensburg
E-mail: janfortlcz@gmail.com, johannes.beer@continental-corporation.com, jens.2.keller@continental-corporation.com
JAN MACEK
Czech Technical University in Prague / Faculty of Mechanical Eng., Center of Vehicles for Sustainable Mobility, Technická 4, 166 07 Praha 6, E-mail: jan.macek@fs.cvut.cz
FREDRIK BORCHSENIUS
Regensburg University of Applied Sciences, Faculty of Mechanical Engineering, Seybothstraße 2, D-93053 Regensburg, E-mail: fredrik.borchsenius@oth-regensburg.de

ABSTRACT
This paper presents a physical, crank angle resolved model of spark ignited (SI) engine process and gas exchange developed by Continental AG for real-time engine management system. Transient 1D flow in pipe systems is the most time-consuming part of the numerical solution. A so-called detailed model, including intake and exhaust pipe components, is defined and reduced to its fast-running version where pipes are neglected. Experimental validation confirms that the detailed model captures transient effects and fulfills accuracy targets over the entire engine operation range, while the fast-running model requires additional empirical parameterization. Both models, however, provide more detailed information on dynamic gas exchange process and the in-cylinder state for each individual engine cycle than today's data driven models do (e.g., transient gas states and internal engine exhaust gas recirculation). Finally, simplifications according to classical acoustic theory are proposed for pipe components to solve the conflict between accuracy and real-time capability.
KEYWORDS: ENGINE MODEL, GAS EXCHANGE, 1D/0D, ECU, REAL-TIME

SHRNUTÍ
Tento článek prezentuje fyzikální model čtyřdobého procesu a výplachu zážehového spalovacího motoru. Model byl vyvinut u Continental AG pro účely sériových řídících jednotek. Nestacionární 1D proudění v potrubních systémech je časově nejnáročnější součástí numerického řešení. Proto je nejprve definován podrobný model, zahrnující řešení sacích a výfukových potrubí, který je dále zjednodušen na rychle fungující verzi se zanedbáním zákona zachování impulsu v potrubních systémech. Experimentální ověření potvrzuje, že podrobný model zachycuje přechodové jevy a splňuje cíle přesnosti v celém rozsahu provozu motoru, zatímco zjednodušený model vyžaduje další empirickou parametrizaci. Oba modely však poskytují podrobnější informace o výplachu a termodynamickém stavu ve válcích než to činí běžné datově orientované modely (např. přechodné stavy plynu, nebo vnitřní recirkulace výfukových plynů motoru). Nakonec jsou navržena zjednodušení řešení proudění v potrubích podle klasické akustické teorie s cílem vyřešení rozporu mezi přesností a schopností dosáhnout řešení v reálném čase na daném hardwaru (ECU 240 MHz).
KLÍČOVÁ SLOVA: MODEL MOTORU, VÝMĚNA NÁPLNĚ VÁLCE, 1D/0D, ECU, REAL-TIME

1. WHY PHYSICAL MODELING INSTEAD OF DATA DRIVEN MODELS?
For spark ignited engines, torque control is realized in the Engine Control Unit (ECU) by managing the in-cylinder air mass, while keeping the air-fuel ratio stoichiometric in order to minimize exhaust emissions. Future CO_2 emission legislation is causing a growing complexity of the engine's gas exchange system. In other words, the number of actuators is increasing. From a modeling perspective, it follows that additional degrees of freedom have to be covered.

In principle, there are two modeling methods: 1. data driven models and 2. physical models, relying on fundamental physical

laws and natural constants. The simplest example of data driven models are look-up tables, which are very efficient in view of CPU performance. However, the memory used is increasing exponentially with the number of model inputs. This resulted in the development of polynomial approximation models and neural networks (e.g. LMN, LOLIMOT [1] [2] [3]) with an increased level of physical based description. These modeling methods are widely used in today's ECUs. Nevertheless, they remain still being data driven models, and therefore, become ineffective when used on complex engine configurations in terms of memory and calibration effort. One way to overcome the limitation of data driven models is the use of physical models describing the engine and gas exchange processes based on the solution of differential equations during engine operation [4] [5] [6] [7].

This paper presents a crank angle resolved real-time engine and gas exchange model for a turbocharged spark ignited (SI) engine developed by Continental AG. Chosen methodology can cover different engine configurations due to its modular structure. Main model outputs are the in-cylinder air and residual gas mass fractions for each single combustion event in addition to the states of the gas exchange system such as the exhaust back pressure and the turbocharger rotational speed. The knowledge of the in-cylinder state for each single combustion event allows a more efficient and emission optimized process control of the engine. For example, the ignition angle set point can be pre-controlled in a more accurate way based on the knowledge of the in-cylinder air mass.

2. THE ENGINE DEVELOPMENT PLATFORM

The model development and experimental investigations are based on a commercial 1.8 liter, 4 cylinder, turbocharged SI-engine. The relevant gas exchange actuators are:

- Throttle valve
- Boost pressure actuator (wastegate) at the turbocharger
- Continuous variable valve timing (CVVT) on intake and exhaust side
- 2-stage variable exhaust valve lift (VVL)
- 2-stage port flap in intake manifold

Recorded actuator positions define the later model inputs. The later model validation is based on the measured in-cylinder air mass in specified engine operating conditions. Signals from above listed actuators are transformed into effective flow areas in related components. Port flap actuator is considered mainly for its influence on flow resistance in air path. Two stages of port flap are represented with two cross sectional areas at opened and closed port flap. Influence on combustion heat release in cylinder is considered indirectly by precalibrated parameters for Vibe combustion model (map-based approach dependent on operating point).

Intake (p_2) and exhaust (p_3) pressures are measured with piezo-resistive absolute pressure sensors (type Kistler 4050, Kulite EWCT-312) with a 1° crank angle resolution. In-cylinder pressure is measured with piezoelectric relative sensors (type Kistler 6041A) also with a 1° crank angle resolution. Thermocouples on both intake and exhaust side are used to measure gas temperature. The engine testing was done under steady state and transient operating conditions.

3. SI-ENGINE PROCESS AND GAS EXCHANGE MODEL

Engine components, such as cylinders, valves, pipes or manifolds are defined separately by sets of Ordinary Differential Equations (ODEs). This enables modular composition of the complete engine gas exchange system. The numerical realization requires a hardware capability to calculate floating point arithmetic.

Mathematical formulation of an explicit system of ODEs

$$\dot{q}=f_{ODE}(t,q) \quad , \quad q=(q_1,q_2,\ldots,q_n) \tag{1}$$

is used to compound the sets of ODEs for each component into one column vector for the entire engine model. The equations are resolved in time by using the explicit 2nd order Runge-Kutta integration method. The model uses a global ODEs solver with a constant integration time step for all model components.

At the beginning, a detailed model was defined to fulfill accuracy targets. This detailed model, including eleven '1D-Pipe' components, is represented by 238 ODEs. The pipe component has dominating influence on CPU load (see section 3.2). For this reason, the model was reduced to its fast-running version, resulting in 73 ODEs.

The number of equations needed for each component of the 4-cylinder engine is summarized in following table:

In the following, the single model components of Tab. 1 are explained.

TABLE 1: Overview of model components and solved differential equations
TABULKA 1: Přehled součástí modelu a řešených diferenciálních rovnic

Number of model components	Number of solved ordinary differential equations	
	Detailed(1D) ∑238 ODEs	Fast-running(0D) ∑73 ODEs
8 x 0D-Volume	8 x 4 = 32 ODEs	8 x 4 = 32 ODEs
4 x 0D-Cylinder	4 x 4 = 16 ODEs	4 x 4 = 16 ODEs
16 x Orifice	16 x 1 = 16 ODEs	16 x 1 = 16 ODEs
1 x Turbocharger	1 x 3 = 3 ODEs	1 x 3 = 3 ODEs
…other	6 x 1 = 6 ODEs	6 x 1 = 6 ODEs
11 x 1D-Pipe	33 elements x 5 = 165 ODEs	… all removed

Basic approach for the engine process is the classic filling-emptying method. The thermodynamic '0D-Volume' is used mainly for manifolds. Only mass and energy conservation are considered. The gas is divided into three specie components: air, burned fuel and unburned fuel to represent the gas composition. A similar approach is used for the engine cylinder.

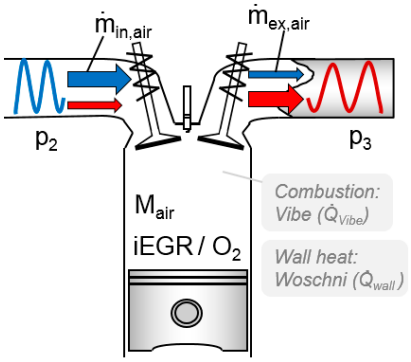

The '0D-Cylinder' is used for the engine cylinder itself, however, has additionally a time-variable volume represented by a look-up table. Fig. 1 shows pulsating mass and energy fluxes, being considered to calculate dynamic equilibrium inside cylinder. Following are four ordinary differential equations (ODEs) that illustrate the change of its thermodynamic gas state:

$$\dot{M}_{air}=\dot{m}_{in,air}-\dot{m}_{ex,air} \tag{2}$$

$$\dot{M}_{Burned} = \dot{m}_{in,Burned} - \dot{m}_{ex,Burned} + \dot{m}_{Vibe} \tag{3}$$

$$\dot{M}_{Unburned}=\dot{m}_{in,Unburned}-\dot{m}_{ex,Unburned}-\dot{m}_{Vibe} \tag{4}$$

$$\dot{U}=h_{in}\,\dot{m}_{in}-h_{ex}\,\dot{m}_{ex}-p_{cyl}\,\dot{V}-\dot{Q}_{Vibe}-\dot{Q}_{Wall} \tag{5}$$

Combustion mass transfer is calculated according to Vibe's empirical model as described in literature [8-page 243]. This model assumes that all unburned fuel inside cylinder burns in one single reaction. Burned mass fraction is defined as ratio of current burned fuel heat to total fuel energy

$$x=\frac{Q_{Vibe}(\phi)}{Q_{B,tot}}=1-e^{\left(c\cdot\left(\frac{\phi-\phi_{BS}}{\Delta\phi_{BD}}\right)^{m+1}\right)} \tag{6}$$

Vibe parameters $c = ln(0.001) = -6.908$ and $m = 2$ are assumed to be constant over entire operating range, whereas crank angle at burn start $\phi_{BS}[°crk]$ and burn duration $\Delta\phi_{BD}[°crk]$ are obtained from calibrated look-up table, dependent on operating point. These parameters were calculated from engine test bench cylinder indication as

$$\Delta\phi_{BD}=CA50-CA10 \tag{7}$$

$$\varphi_{BS} = CA50 - \sqrt[3]{\frac{ln(0.5)}{c}}\cdot\Delta\varphi_{BD} \tag{8}$$

where CA10, CA50 and CA90 are crank angle values at which 10 %, 50 % and 90 % of heat is released, calculated from measured in-cylinder pressure. Heat transfer into cylinder walls is calculated with a Woschni approach [8-page 231]. Thermodynamic properties of combustion gases are approximated with a piece-wise polynomial model using a database published by Grill [9].
Gas exchange actuators (inlet and exhaust valves, throttle, etc.) listed in section 2 are represented by the 'Orifice' component. Signal input from ECU represents the cross-section area of each flow restriction. The 'Orifice' flow is calculated according to Saint-Venant relation for compressible flow [10] using the upstream and downstream pressure from neighboring components. Intake and exhausted valve discharge coefficients were obtained from air flow test bench measurement.
The 'Turbocharger' component is represented by a look-up table-based model. It is extended by a differential equation for rotational mass to consider dynamic inertia effects. Data for compressor and turbine are obtained from a turbocharger stationary hot-gas test bench.
Flow in intake and exhaust pipe systems, including wave propagation and gas inertia effects, is represented in the '1D-Pipe' component being discretized in space Δx (explained in section 4 in more detail).

3.1 SI-ENGINE PROCESS AND GAS EXCHANGE MODEL

To fulfill the control objectives, exact prediction of in-cylinder air mass is of key importance. Measured in-cylinder air mass was calculated from injected fuel and current air-fuel ratio. Air-fuel ratio was estimated from Brettschneider equation. Additionally, scavenging mass is considered in dependence on measured CO/CO_2 ratio to calculate in-cylinder trapped mass. This is done by an assumption for trapping efficiency based on regression fit of data from similar reference engine [13], [14]. Model accuracy is then estimated in every operating point as the percentage-error between measured and simulated in-cylinder air mass.

Percentage-error:

$$PE(@N/IMEP)=\frac{M_{air}(Simulation)-M_{air}(Measurement)}{M_{air}(Measurement)}\ x\ 100\% \tag{9}$$

Overall accuracy of 240 measured operation points is defined as the „Root Mean Square Error":

Air-mass-error:

$$RMSE = \sqrt{\frac{1}{n}\cdot\sum_{i=1}^{n} PE_i^{\,2}} \tag{10}$$

Comparison of the full engine operating range in steady state experiments with the detailed model results in an overall air-mass-error of RMSE = 5.7%err (see Fig. 2-Left). Highest model deviations occur at low engine load. This is to be expected due to the fact that accuracy criterium is a relative deviation with denominator M_{air}, being smaller at low loads. Accuracy requirement 5%err allows 45 mg deviation at full load points with $M_{air,} = 900\,mg$, but allows only 5 mg deviation at lowest loads with measured $M_{air,} = 100\,mg$. Beside this, loads with $IMEP < 2\ bar$ have higher cycle to cycle deviation (Covariance of standard deviation of $IMEP$ is 5 % at $IMEP < 2\ bar$, but it is only 1,5 % in other operating points). To improve accuracy at low loads, more complex model calibration would be required. For example, current model assumes that 100 % of fuel burns inside of cylinder. In reality, part of the fuel burns outside cylinder, which is characterized by combustion efficiency. Emission based combustion efficiency of measured engine varies between 90 % and 98 %. This fact may explain part of the unexpected model deviations and should be considered in future. Another source of deviations is the numerical discretization. While the numerical solver is time based, higher integration time steps become limiting for calculation of crank angle dependent engine process. Integration time step of $\Delta t = 300$ µm corresponds to 1.5 degree at 850 rpm, but the resolution at maximum engine speed of 6000 rpm becomes with 11 degree quite inaccurate.

Fig. 2-Right shows the comparison of both detailed and fast--running models with the exhaust pressure sensor in a selected turbocharged operating point. Intake (IN) and exhaust (EX) valve opening areas, as well as the top dead center (TDC), are marked gray in Fig. 2-Right. The amplitude of pressure pulsations p_3 is very high in comparison to its mean value. Both models provide qualitatively realistic exhaust pressure pulsations in comparison to measurements. This shows the potential of physical modeling, for example to improve the boost pressure control, when used instead of classical mean value models.

The accuracy results are obtained with the use of a global model parameterization, valid for the entire engine operating range. Geometrical engine parameters such as valve effective flow areas and discharge coefficients, heat transfer coefficients, etc. are not recalibrated. However, the fast-running model cannot provide correct boundary conditions for the cylinders without additional empirical parameterization. Moreover, the exhaust valve mass flow in fast-running model was stabilized due to numeric issues. The stabilization is based on 1st order differential equation added to the Saint-Venant 'Orifice' flow. This causes an unwanted time delay in exhaust pressure dynamics by the fast-running model (see Figure 2, Right). The air-mass-error of fast-running model is RMSE=7.4%err. Due to this problem, the fast-running model would require higher calibration effort to reach the accuracy objectives.

The detailed model shows a better model accuracy than the fast--running model. Besides the model accuracy, real-time capability is crucial.

3.2 EVALUATION OF REAL-TIME CAPABILITY

A multicore Engine Computational Unit (ECU) with a clock frequency of 240MHz, capable of calculating floating point arithmetic, was used as a validation platform. Figure 3 illustrates necessary conditions to fulfill the real-time capability:

Engine management system expects model results at the end of every ECU sample period. Therefore, the processor (CPU) has to be able to finish model execution by the end of the ECU sample period. This is expressed by the definition of real-time factor RT as a ratio of the CPU time to the ECU sample period.

Necessary CPU time for one integration time step of the ODEs solver was estimated offline by analyzing each model component.

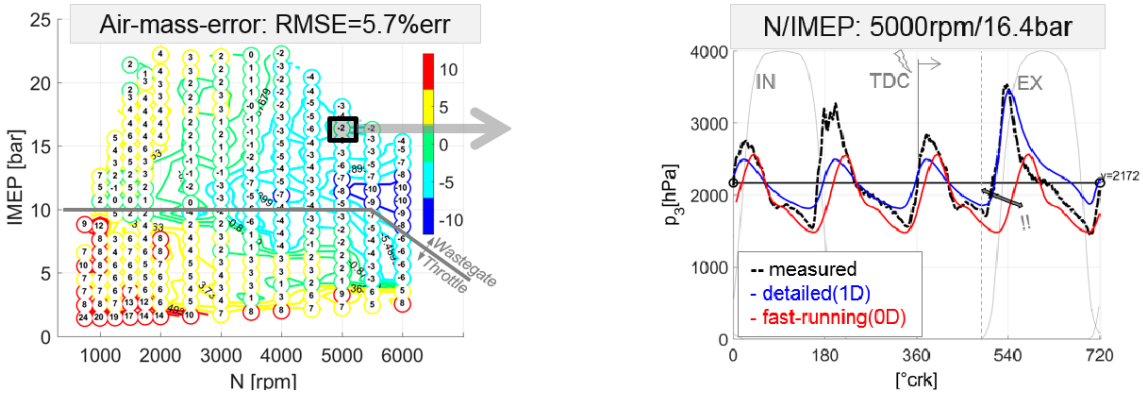

FIGURE 2: Left: Engine map of detailed model providing PE in every measured steady state operating point resulting in an air-mass-error of RMSE = 5.7%err. Right: Exhaust pressure pulsations p3 of detailed model and fast-running model compared to Kulite EWCT-312 sensor

OBRÁZEK 2: Vlevo: Mapa motoru v detailním modelu, zobrazující PE v každém měřeném stacionárním bodě. Výsledná odchylka v hmotnosti vzduchu RMSE = 5.7%err. Vpravo: Tlakové pulzace p_3 ve výfuku, detailní model a fast-running model, porovnání s měřením senzorem Kulite EWCT-312

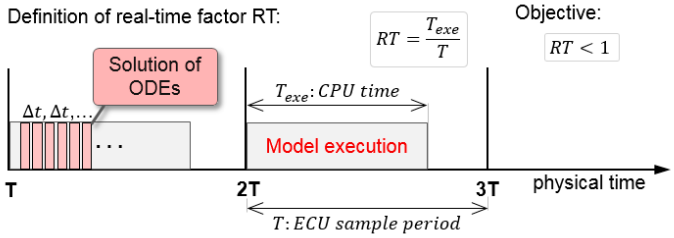

FIGURE 3: Real-time control timing on ECU
OBRÁZEK 3: Časování v ECU v reálném čase

The offline estimation is based on the sum of the mathematical operations involved (additions/subtractions, multiplications, divisions, etc.) in the code, and taking into account the integration time step size used. This offline estimation was validated by implementation of the fast-running model on the target hardware.

The detailed model requires a small integration time step of $\Delta t = 30$ µs to satisfy the Courant-Lewy-Friedrichs ($FL = \frac{c \cdot \Delta t}{\Delta x}$) stability condition in the exhaust pipe. This results in a very high real-time factor of RT = 43. Simulation could be ten times faster with a time step $\Delta t = 300$ µs so as the real-time factor becomes RT = 4.3 (see Fig. 4-Blue). However, the simulation is then unstable. Neglecting spatial resolution by removing of all '1D-Pipe' components results in the fast-running model and enables a stable calculation with a relatively high time step $\Delta t = 300$ µs. The calculation of fast-running model components results in a real-time factor of RT = 1.9 (see Fig. 4-Red). Fig. 4 shows the computational demand of components in both detailed and fast-running model (see also Tab. 1) estimated with an assumption of the same time step.

The dashed line represents the development target for the complete engine model. Sum of all component RT factors results in the RT factor of the entire model. The eleven '1D-Pipe' components would alone be 2.5 times beyond real time capability. This makes the complex 1D flow approach (explained in section 4.1) of the so-called detailed model not feasible for the real time implementation on target hardware.

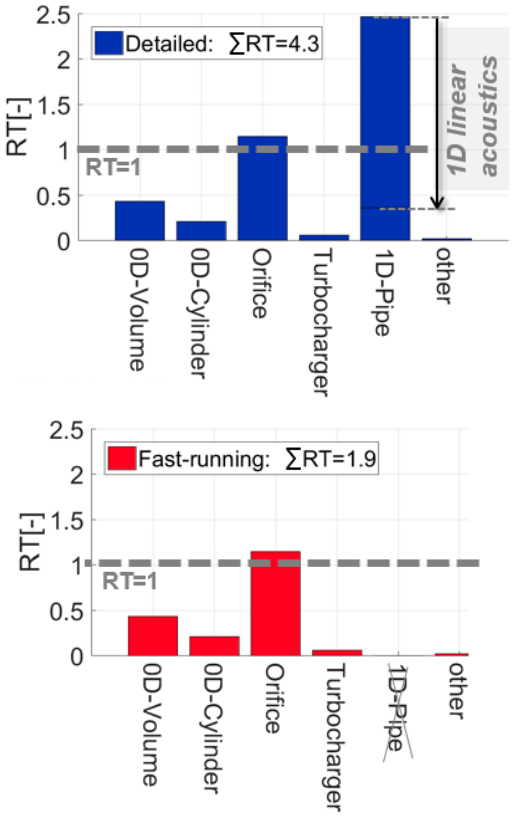

FIGURE 4: Processor load by calculation of
Upper: detailed model (237 ODEs, ∑RT = 4.3) with assumption of instable time step Δt = 300 µs. Lower: fast-running model (72 ODEs, ∑RT = 1.9) with a stable time step Δt = 300 µs
OBRÁZEK 5: Zatížení procesoru výpočtem
Horní: detailního modelu (237 ODR, ∑RT = 4.3) s předpokladem nestabil. časového kroku Δt = 300 µs. Dolní: *Fast-running model* (72 ODR, ∑RT = 1.9) se stabilním časovým krokem t = 300 µs.

3.3 CONFLICT BETWEEN ACCURACY AND REAL-TIME CAPABILITY

Following graph illustrates results achieved and presented above in this paper:

Again, the dashed line represents the development target. Target model accuracy is a cylinder air-mass-error RMSE<5%err being less than five percent over the engine operating range.

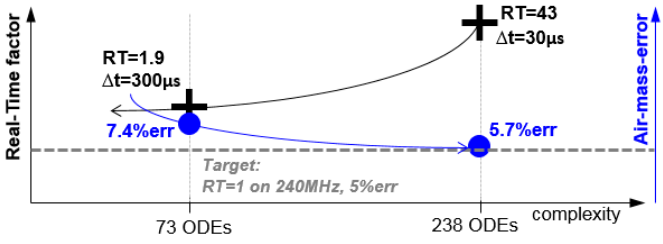

FIGURE 5: Air-mass-accuracy and real-time factor of the fast-running model versus the detailed model
OBRÁZEK 5: Přesnost určení průtoku vzduchu a real-time faktoru pro fast running model a detailní model

Under some assumptions, the fast-running model (73 ODEs) has already a potential to be real-time capable on future ECUs, for example when the CPU clock frequency increases to ~350MHz as stated in [12]. But the air-mass-error is not satisfying yet. Sufficient accuracy is achieved by modelling of an engine gas exchange system in more detail, but it causes a conflict with the real-time capability. CPU time increases with space resolution and with the number of needed ODEs. The detailed model with a sufficient accuracy of RMSE = 5.7%err is stable only using a time step $\Delta t \leq 30$ µs. This model would need 43 times more processor performance to be real-time capable.

4. OPTIMIZATION OF THE '1D-PIPE' COMPONENT

The objective is to find the simplest possible approach to allow the calculation of pressure wave propagation through space, especially with unstable momentum conservation. The accuracy issues are not considered primarily.

4.1 COMPLEX TRANSIENT 1D FLOW IN PIPES

The 1D flow in the detailed model is described by the complete set of three transport conservation laws for mass, momentum and energy. Governing equations can be taken from Pischinger [10-page 30]. Mass conservation is formulated for all three gas components: air, burned fuel and unburned fuel. Empirical source terms for wall friction and heat transfer are considered. Caloric properties of the gas mixture are assumed to be a function of temperature and air-fuel ratio. The single pipe component is assumed to have constant cross-sectional area. Partial Differential Equations (PDEs) are discretized in space by using 1st order upwind scheme on a 1D finite volume mesh leading in a set of Ordinary Differential Equations (ODEs). This differential scheme is computationally very fast; however, it requires additional numerical stabilization. The use of explicit time integration methods (2nd order Runge-Kutta), especially in combination with long integration time steps, leads to numerical oscillations. Numerical stabilization was formulated as a function of element gas velocities by using a simple spring-damper model. The complex pipe model provides quite detailed information on thermal transport effects, though its complexity does not enable real-time capability on a current ECU.

4.2 SIMPLIFICATION TO 1D LINEAR ACOUSTICS

The complex '1D-Pipe' approach is changed as follows:

- Governing equations: All three conservation laws (nonlinear) → Linearized acoustic equations
- Discretization scheme: Upwind → Riemann solver
- Caloric gas properties: Variable → Constant

Classical acoustic theory provides a reasonable compromise to consider basic pressure wave propagation while reducing the computational time [6] [7] [10-page 33]. Constant gas properties reduce the computational time further. Change of the discretization scheme improves numerical stability.
Simplifications according to classical acoustic theory [10-page 31] [11-page 26] are taken into account:

$$u \ll c \left[\frac{m}{s}\right]$$

… Flow velocity is small in comparison to local speed of sound

$$\rho \sim \bar{\rho} \left[\frac{kg}{m^3}\right]$$

… Small density oscillation around its given mean value

$$\dot{q} = 0 \left[\frac{W}{kg}\right]$$

… Adiabatic state changes (zero heat transfer)

$$T = \bar{T}\,[K] \rightarrow \bar{c} = \sqrt{\kappa R \bar{T}} \left[\frac{m}{s}\right]$$

… Temperature is constant and given. This results in constant local speed of sound
Thermodynamic gas properties are calculated only once at the initial time step for a given reference temperature. The simplified transport equations can be written in matrix form using the state q, linearized flux $f = A \cdot q$ and a source term s

$$q_t + f(q)_x = s \tag{11}$$

$$\begin{bmatrix} p \\ u \end{bmatrix}_t + \begin{bmatrix} 0 & \bar{\rho}\bar{c}^2 \\ 1/\bar{\rho} & 0 \end{bmatrix} \cdot \begin{bmatrix} p \\ u \end{bmatrix}_x = \begin{bmatrix} 0 \\ a_{fric} \end{bmatrix} \tag{12}$$

$$a_{fric} \left[\frac{m}{s^2}\right] = \frac{-\Delta p_f}{\Delta x \cdot \bar{\rho}} \tag{13}$$

The only state variables are pressure and velocity u. The source term considers empirical wall friction. Solution is obtained by using a so-called Riemann solver, which calculates the middle flux on the cell boundary „i+1/2" depending on left „L=i" and right „R=i+1" neighboring states. Due to the linearity of matrix A, it is possible to estimate only the middle state on the cell boundaries. Then the middle flux is easily given by $f_{i+1/2} = A \cdot q_{i+1/2}$
Equation for middle state can be taken from LeVeque [11-page 57]

$$\begin{bmatrix} p_{i+1/2} \\ u_{i+1/2} \end{bmatrix} = 0.5 \cdot \begin{bmatrix} (p_i + p_{i+1}) + \bar{\rho}\bar{c} \cdot (u_i - u_{i+1}) \\ (u_i + u_{i+1}) + 1/\bar{\rho}\bar{c} \cdot (p_i - p_{i+1}) \end{bmatrix} \tag{14}$$

Static pressure is assumed to be known (for example from a neighboring '0D-Volume' component) at the left boundary condition $p_{0+1/2} = p_{BL}$ and velocity (for example from a neighboring 'Orifice' component) at the right boundary condition $u_{N+1/2} = u_{BR}$.
Equations for left and right boundary elements are

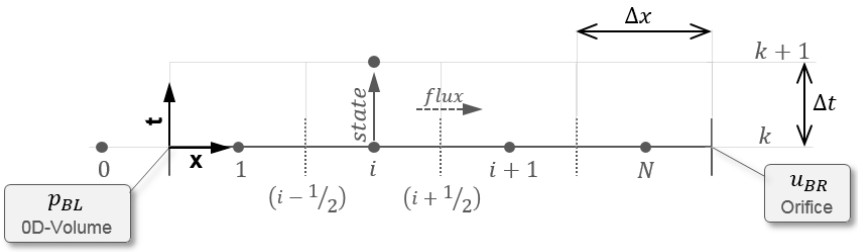

FIGURE 6: Time-space domain, upper index „k" is used for time and the lower index „i" for space iteration
OBRÁZEK 6: Časoprostorová oblast, horní index „k" odpovídá času, dolní index „i" odpovídá prostorovému kroku

$$\begin{bmatrix} p_{0+1/2} \\ u_{0+1/2} \end{bmatrix} = \begin{bmatrix} p_{BL} \\ u_1 + 1/\bar{\rho}\bar{c} \cdot (p_{BL} - p_1) \end{bmatrix} \quad (15)$$

$$\begin{bmatrix} p_{N+1/2} \\ u_{N+1/2} \end{bmatrix} = \begin{bmatrix} p_N + \bar{\rho}\bar{c} \cdot (u_N - u_{BR}) \\ u_{BR} \end{bmatrix} \quad (16)$$

Next „Finite Volume Method" discretization of state and flux vectors

$$\frac{q_i^{k+1} - q_i^k}{\Delta t} + \frac{f_{i+1/2}^k - f_{i-1/2}^k}{\Delta x} = s \quad (17)$$

is used to resolve variables in time and space. The space resolution is calculated by the pipe component itself. On the other hand, the time integration is implemented into the global ordinary differential equations solver (2nd order Runge-Kutta) using following equation for the change of gas state:

$$\dot{q}_i = \frac{1}{\Delta x} \cdot \left(f_{i-1/2}^k - f_{i+1/2}^k \right) + s \quad (18)$$

$$\begin{bmatrix} \dot{p}_i \\ \dot{u}_i \end{bmatrix}_{FVM} = \frac{1}{\Delta x} \begin{bmatrix} \bar{\rho}\bar{c}^2 \cdot \left(u_{i-1/2} - u_{i+1/2} \right) \\ 1/\bar{\rho} \cdot \left(p_{i-1/2} - p_{i+1/2} - \Delta p_{fric} \right) \end{bmatrix} \quad (19)$$

This formulation results in an identical time step for all thermodynamic volume elements formulated by the filling-emptying approach and acoustical pipe elements. It is also possible to formulate locally different integration time step. Wall friction Δp_{fric} is calculated as a function of Reynolds number.

4.3 DISCUSSION AND EXPECTED BENEFITS

Both numerical methods used in the complex (section 4.1) and the simplified acoustic (see section 4.2) '1D-Pipe' component were tested for stability by defining discontinuous initial value problems (so called Riemann problems) and compared to their exact analytical solution. The Riemann solver used in the simplified pipe provides better stability with fewer grid points than the previously used upwind scheme. Therefore, higher critical CFL number can be used. Maximum potential of presented simplifications when applied on all pipe components in detailed model results in a real-time factor RT=2.2 (see Fig 4.).

Expected accuracy benefit in intake manifold components upstream of a throttle valve, and downstream of a turbocharger, is a part of current investigations. The presented approach has to be extended by energy conservation (also linearized) and formulated for entire gas composition (e.g., air, burned fuel, unburned fuel) to be able to capture transport problems in the primary intake and exhaust runners directly connected to cylinders.

5. CONCLUSION

The engine process and gas exchange were described with the use of 238 ODEs in the detailed model, providing all necessary information for control purpose of the selected 1.8 L, 4-cylinder SI-engine.

The model was simplified to its fast-running version but lacking the required model information. The model real-time factor of RT = 1.9 is close to real time capability on the serial ECU equipped with a microprocessor of 240MHz clock frequency.

Ongoing research activities to reduce numerical effort for the CPU time consuming 1D pipe components are discussed. The complex approach for calculating all three transport conservation laws was simplified by using assumptions from classical linear acoustic theory. Calculating of momentum conservation causes significantly lower processor load and remains numerically stable even for large integration time steps.

The newly developed model is capable of providing more information than state-of-the-art ECU models (such as internal engine exhaust gas recirculation, in-cylinder air mass, as well as transient gas states in the complete engine's gas exchange system). Because of physical air path modelling (based on natural laws and constants), the calibration effort and required memory space does not increase exponentially with engine complexity. If the future ECU processor performance is constantly increasing as it has in the last couple of years, (as stated for example in [12]) it makes the newly developed model interesting for implementation in next generation ECUs.

REFERENCES

[1] Kainz, J.; Beer, J.; Bänfer, O; Nelles, O. Einsatz von lokalen Modell-Netzen in einer Motorsteuerung zur Modellierung von Ventiltriebsvariabilitäten, Congress „Haus der Technik" variable Ventilstewuerung, Essen, 2009

[2] Macek, J.; Polasek, M.; Sika, Z.; Valasek M.; Florian M.; Vítek O. Transient Engine Model as a Tool for Predictive Control, Czech Technical University in Prague, SAE 2006-01-0659

[3] Nelles, O.; Bänfer, O.; Kainz, J; Beer, J. Local Model Networks, In: The Prospective Method for Modeling in Electronic Control Units? ATZelektronik 06I2008

[4] Wurzenberger, J.; Reinzle, R.; Schuemie, A.; Katrasnik, T. Crank-Angle Resolved Real-Time Engine Simulation – Integrated Simulation Tool Chain from Office to Testbed, SAE 2009-01-0589

[5] Friedrich, I". Motorprozess-Simulation in Echtzeit – Grundlagen und Anwendungsmöglichkeiten, TU-Berlin, Sharker Verlag Aachen, Berlin, 2008, ISBN 987-3-8322-7019-3

[6] Roesler, C.; Echtzeitfähiges physikalisches Motorprozessmodell – Potenziale für die Steuerung eines Pkw-Ottomotors, Technical University of Berlin, Berlin, 2013, ISBN 978-3-8325-3359-5

[7] Ludwig, O.; Eine Möglichkeit zur echtzeitfähihen, physikalisch-basierten Motorprozessanalyse auf der Grundlage zeitlich fusionierter Messdaten, Logos-Verlag Berlin, Hamburg, 2011, ISBN 978-3-8325-2792-1

[8] Merket, P.; Schwarz, CH. Grundlagen Verbrennungsmotoren; Simulation der Gemischbildung, Verbrennung, Schadstoffbildung und Aufladung, Vieweg +Teubner, Wiesbaden, 2009, ISBN 978-3-8348-0740-3

[9] Grill, M. Objektorientierte Prozessrechnung von Verbrennungsmotoren, Institut für Verbrennungsmotoren und Kraftfahrwesen der Universität Stuttgart, Stuttgart, 2006

[10] Pischinger, R.; Kell, M.; Sams, T. Thermodynamik der Verbrennungskraftmaschine, Springer Verlag, Wien, 2009, ISBN 978-3211-99276-0

[11] LeVeque, Randall J. Finite Volume Methods for Hyperbolic Problems, University of Washington, Cambridge University Press, Cambridge, 2004, ISBN 0-511-04219-

[12] Borean, F.; Message, S.; Morgan, CH.; Neaves B.; Slaney, T.; Jaguar Land Rover, Coventry, UK 2020-2025 Challenges for Combustion Control in Automotive World: Hybridization, Emissions and Key Enablers, Symposium for Combustion Control 2016, Aachen

[13] Beer, J.; Koch, A. Injection and IVVT-Strategy to Improve the Behavior of a Turbocharged Engine with Direct Injection, Siemens VDO Automotive AG, Regensburg, 2003

[14] Huber, E. W. Measuring the Trapping Efficiency of Internal Combustion Engines Through Continuous Exhaust Gas Analysis, Institut fuer Motorenbau, Detroit, 1971, SAE-710144